SrTiO₃(001)(2×1) reconstructions: First-principles calculations of surface energy and atomic structure compared with scanning tunneling microscopy images

Karen Johnston,* Martin R. Castell,[†] Anthony T. Paxton, and Michael W. Finnis
*Atomistic Simulation Group, Department of Pure and Applied Physics, Queen's University Belfast,
Belfast BT7 1NN, Northern Ireland, United Kingdom*
(Received 23 February 2004; published 26 August 2004)

(1×1) and (2×1) reconstructions of the (001) SrTiO₃ surface were studied using the first-principles full-potential linear muffin-tin orbital method. Surface energies were calculated as a function of TiO₂ chemical potential, oxygen partial pressure and temperature. The (1×1) unreconstructed surfaces were found to be energetically stable for many of the conditions considered. Under conditions of very low oxygen partial pressure the (2×1) Ti₂O₃ reconstruction [Martin R. Castell, Surf. Sci. **505**, 1 (2002)] is stable. The question as to why STM images of the (1×1) surfaces have not been obtained was addressed by calculating charge densities for each surface. These suggest that the (2×1) reconstructions would be easier to image than the (1×1) surfaces. The possibility that the presence of oxygen vacancies would destabilise the (1×1) surfaces was also investigated. If the (1×1) surfaces are unstable then there exists the further possibility that the (2×1) DL-TiO₂ reconstruction [Natasha Erdman *et al.* Nature (London) **419**, 55 (2002)] is stable in a TiO₂-rich environment and for $p_{O_2} > 10^{-18}$ atm.

I. INTRODUCTION

General interest in the properties of metal oxide crystal surfaces has emerged from such diverse fields as catalysis, corrosion, microelectronics, and gas sensing.[1] Surface studies on SrTiO₃ crystals in particular are relevant to applications involving thin film growth where they are commonly used as a substrate. Exploitation of the dielectric properties has stimulated research into the creation of SrTiO₃ thin films. Knowledge of the atomic scale structure of the surfaces is central to developing a fundamental understanding of SrTiO₃ properties especially those related to very thin film growth where the nature of the interface is significant.

The unreconstructed (001) surface of perovskite SrTiO₃ has two possible charge neutral terminations. Due to their stoichiometry the terminations are referred to as the TiO₂ and SrO surfaces. Numerous reports of surface studies on the (1×1) terminations exist, and indeed our first principles calculations in this paper show that they have low energy and are expected to be very stable. The traditional picture of the unreconstructed (001) surface is of (1×1) regions of TiO₂ and SrO terminations separated by half unit cell height steps as shown in Fig. 1(a). Surprisingly there are no atomic resolution scanning tunneling microscopy (STM) images of this type of surface termination. It is possible to create clean flat surfaces of SrTiO₃ (001) with large terraces but when imaged in the ultra high vacuum (UHV) environment of the STM they are always reconstructed in some form and only have one type of termination with full unit cell height steps. STM images of the (2×1), $c(4 \times 4)$, $c(2 \times 4)$, $c(6 \times 2)$, and (6×2) reconstructions have been reported in the literature.[2–5] UHV transmission electron microscopy (TEM) analysis of the (2×1) and $c(2 \times 4)$ reconstructions have also been published.[6,7] In this paper we will focus on the possible origin and structure of the (2×1) surface and discuss the

possibility that there may be more than one reconstruction with a (2×1) surface unit cell.

The three candidate structures that currently exist for the (2×1) reconstruction are shown in Figs. 1(b)–1(d). In Fig. 1(b) alternate rows of oxygen have been removed from the TiO₂ terminated (1×1) surface to create a (2×1) surface with a reduced surface stoichiometry of Ti₂O₃ and it will therefore be referred to in this paper as the (2×1) Ti₂O₃ surface.[4] Figure 1(c) shows a proposed structure with reduced surface coverage of Ti but maintaining the TiO₂ stoichiometry and will be called the (2×1) TiO₂ surface.[4] A further possibility proposed by Erdman *et al.*[6] is shown in Fig. 1(d). It is an unusual structure in that the surface has a double layer TiO₂ termination and it will be referred to as the (2×1) DL-TiO₂ surface. Reconstructions that are SrO terminated are not considered here as most experimental data indicate a Ti rich termination.

Kubo and Nozoye[8] have recently made the interesting suggestion that reconstructions observed can be explained as arising from patterns of Sr adatoms on a TiO₂ terminated (1×1) surface, although this has not been backed up by free energy calculations.

Given the stability of the (1×1) surfaces, why then are there no atomic resolution STM images? There are two likely explanations. The (1×1) terminations may simply be too electronically flat to allow atomic resolution STM imaging which is the reason postulated for the difficulty in obtaining atomic resolution images of CoO (001) (1×1).[9] Alternatively, the SrTiO₃ (1×1) terminations might simply not be stable in a realistic UHV experiment. When preparing a crystal to examine its surface atomic layer it must be clean and ordered. To produce a surface free of adsorbates it is necessary to anneal it in UHV conditions which in turn will encourage surface oxygen defects to be created. We show in this paper that under certain conditions a (2×2) unit cell
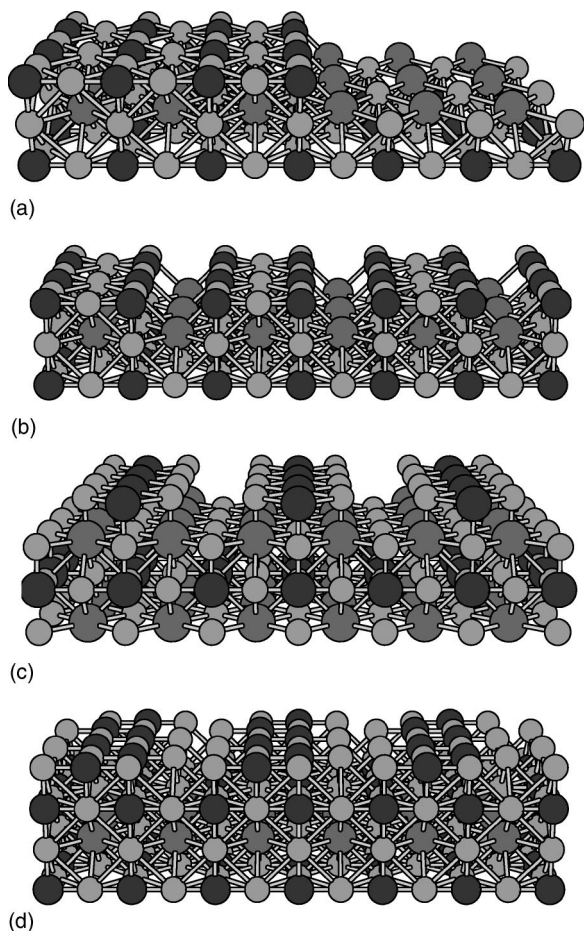
FIG. 1. (a) (1×1) unreconstructed TiO_2 and SrO surfaces. (b) (2×1) Ti_2O_3 reconstruction. (c) (2×1) TiO_2 reconstruction. (d) (2×1) DL-TiO_2 reconstruction. Ti atoms are darkest and O are lightest.

with a missing oxygen atom has a higher surface energy than the (2×1) reconstructions. It is therefore quite possible that a perfect (1×1) termination is stable in UHV conditions, but as soon as an oxygen atom is lost into the vacuum this results in local (2×1) ordering which in turn causes more oxygen loss and hence more (2×1) ordering. A clean surface with large (1×1) terraces suitable for UHV STM imaging will therefore rapidly reconstruct to a (2×1) surface.

The paper is organized as follows: Sec. II describes the method of total energy calculations. Section III describes in detail the theory used to treat nonstoichiometric surfaces and includes a derivation of the temperature and pressure dependence of the chemical potential of oxygen. The results of surface relaxations, surface energies and charge densities are presented in Sec. IV and V as well as a discussion of their implications. The final section summarizes the main conclusions of this work.

II. METHOD OF TOTAL ENERGY CALCULATIONS

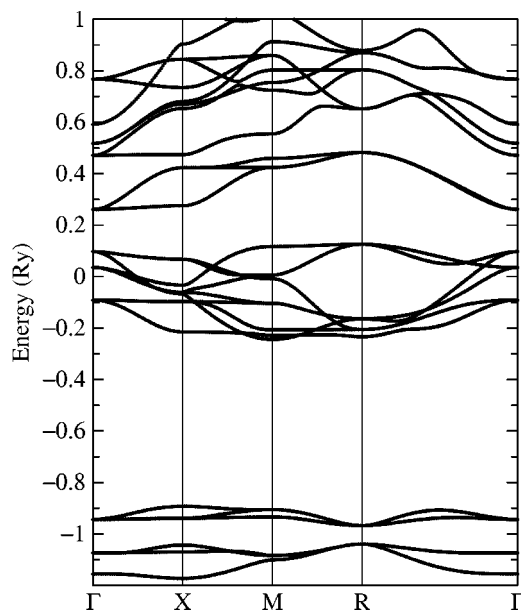We have used the full-potential linear muffin-tin orbitals (FP-LMTO) method written by Methfessel and van

FIG. 2. FP-LMTO band structure of $SrTiO_3$.

Schilfgaarde.[10,11] This method implements density functional theory within the local density approximation (LDA). We have not included gradient corrections to the LDA exchange and correlation functional. This would not add to the computation time, but we have have found in earlier work on stoichiometric and reduced surfaces of TiO_2 that these do not affect surface energies or structures although they do tend to overestimate the magnetic moment if there are unpaired spins.[12] The basis functions are envelopes of "smooth" Hankel functions (which are convolutions of solid Hankel functions and Gaussians) augmented within atomic spheres with numerical solutions of the radial Schrödinger equation (including scalar relativistic corrections).

For $SrTiO_3$ we have used a basis consisting of Sr $5s, 5p, 4d$, Ti $4s, 4p, 3d$, and O $2s, 2p, 3d$ orbitals. The Sr $4p$ and Ti $3p$ orbitals were included in the basis as "local orbitals".[13] The atomic sphere radii were 2.4 a.u. for Sr, 2.12 a.u. for Ti, and 1.45 a.u. for O. The Sr $4s$ and Ti $3s$ core states were treated with the frozen overlapped core approximation.

For bulk calculations a Brillouin zone mesh of $4 \times 4 \times 4$ and a Fourier transform mesh of $32 \times 32 \times 32$ were used. The calculated electronic bandstructure is shown in Fig. 2. The band gap is approximately 0.13 Ry (1.79 eV) which compares well to the previous calculations in Ref. 14 who obtained a band gap of ≈ 2 eV. The equilibrium lattice constant of $SrTiO_3$ was found to be $a_0 = 3.85$ å and the bulk modulus was $K = 200$ GPa. The elastic constants were $c' = 140$ GPa and $c_{44} = 125$ GPa. The corresponding experimental values are $a_0 = 3.905$ Å,[15] $K = 184$ GPa,[15] $c' = 119$ GPa, and $c_{44} = 128$ GPa.[16] The error between the theoretical values and experimental values are typical of the LDA which tends to overbind the system.

All our calculations of the various surface structures were performed using the theoretical lattice constant. The Brillouin zone mesh and the Fourier transform mesh were scaled to correspond with those used for the bulk unit cell.

Surfaces are represented in our calculations by periodically repeating slabs separated by vacuum having a thickness in the range $1-3$ a_0.

III. THEORY OF NONSTOICHIOMETRIC SURFACES

The theory necessary to compare the free energy of surfaces with different stoichiometries has been described in Refs. 17–19. In this section we summarize the general principles and include a fuller description than before of how to account for the oxygen partial pressure.

Since we are dealing with a two phase system made up of three components, the phase rule tells us that we have three degrees of freedom. It is convenient to choose these to be the chemical potential of TiO_2, the partial pressure of oxygen (equivalent to its chemical potential), and the temperature: μ_{TiO_2}, p_{O_2}, T. With these three parameters specified, the surface excess free energy is calculated for a particular structure and stoichiometry as

$$\sigma(\mu_{TiO_2}, p_{O_2}, T) = \frac{1}{2A_s}\left(G_s - \sum_i \mu_i N_i\right), \quad (1)$$

where G_s is the Gibbs free energy of the slab, N_i is the number of each component i within the slab, and μ_i is the chemical potential of component i per formula unit. A_s is the area of one of the surfaces of the slab and the factor of $\frac{1}{2}$ accounts for the fact that there are two surfaces per slab. The idea is that the predicted surface structure would be the one that minimizes (1). Although the theory implicitly takes into account the temperature and pressure of the oxygen in the vapour phase, the calculations for the solid will be done at a temperature of absolute zero. This approach also leaves out in practice any consideration of either configurational entropy or vibrational entropy associated with the surface structure. The former is not significant for ordered surfaces such as the ones we are dealing with, while the latter error would certainly be significant in deciding between closely competing surface structures.

The surface free energy can also be expressed in terms of the excesses Γ_i of the components. The surface excess Γ_i of component i with respect to component A is

$$\Gamma_i = \frac{1}{A_s}\left(N_i - N_A \frac{N_i^{bulk}}{N_A^{bulk}}\right). \quad (2)$$

We choose component A to be SrO and introduce the surface excesses of TiO_2 and O, in terms of which the surface free energy is now

$$\sigma = \frac{1}{2A_s}(G_s - N_{SrO}g_{SrTiO_3}) - \mu_{TiO_2}\Gamma_{TiO_2} - \frac{1}{2}\mu_{O_2}\Gamma_O, \quad (3)$$

where g_{SrTiO_3} is the Gibbs free energy of a bulk formula unit of $SrTiO_3$. The surface excesses Γ_{TiO_2} and Γ_O for each surface are listed in Table I.

The relative stability of the different surface structures depends on the chemical potentials which are discussed in the following subsections.

TABLE I. Surface excesses of subunits TiO_2 and O with respect to SrO for different surface terminations. $A_s^{(1\times1)}$ is the area of one of the surfaces of a (1×1) terminated slab.

Surface	$A_s^{(1\times1)}\Gamma_{TiO_2}$	$A_s^{(1\times1)}\Gamma_O$
(1×1) TiO_2	$1/2$	0
(1×1) SrO	$-1/2$	0
(2×1) TiO_2	0	0
(2×1) Ti_2O_3	$1/2$	$-1/2$
(2×1) DL-TiO_2	$3/2$	0

A. Chemical potential of TiO_2

We cannot calculate μ_{TiO_2} for the particular conditions under which the observed surface structures were created, but we can put bounds on it by the standard method applied in Ref. 20 as we now describe. For this we introduce $\Delta G_{f,SrTiO_3}^0$, defined as the Gibbs free energy of formation of one formula unit of bulk $SrTiO_3$ with respect to SrO and TiO_2, so that

$$\Delta G_{f,SrTiO_3}^0 = g_{SrTiO_3}^0 - g_{SrO}^0 - g_{TiO_2}^0, \quad (4)$$

where $\Delta G_{f,SrTiO_3}^0 < 0$. $g_{SrTiO_3}^0$, g_{SrO}^0 and $g_{TiO_2}^0$ are the Gibbs free energies of the bulk crystal per formula unit in their standard states and in our work they are approximated by their 0 K total energy. SrO was calculated in the rocksalt structure, TiO_2 in the rutile structure, and $SrTiO_3$ was calculated in the cubic perovskite structure. The difference in energy between the ideal cubic perovskite structure and the relaxed low temperature structure was considered to be insignificant. The formation energy was calculated to be $\Delta G_{f,SrTiO_3}^0 = -0.1094$ Ry.

The equilibrium of the slab requires that

$$g_{SrTiO_3} = \mu_{SrO} + \mu_{TiO_2}. \quad (5)$$

Neglecting the temperature dependence and stoichiometry variation of the free energy of bulk $SrTiO_3$, then $g_{SrTiO_3} = g_{SrTiO_3}^0$ and

$$\mu_{SrO} + \mu_{TiO_2} = g_{SrTiO_3}^0, \quad (6)$$

which confirms explicitly that only one of these chemical potentials is an independent degree of freedom. Neither μ_{TiO_2} nor μ_{SrO} can be predicted in the system under study, because the equilibrium conditions prevailing at the surface are not known. However it is known that

TABLE II. Standard oxygen chemical potential $\mu_{O_2}^0$ in Ry, (a) from Gibbs energies, and (b) from enthalpies.

	(a)	(b)
TiO_2		-0.616
SrO	-0.622	-0.624
Al_2O_3	-0.614	-0.608

$$\mu_{\text{TiO}_2} \leq g^0_{\text{TiO}_2}, \tag{7a}$$

$$\mu_{\text{SrO}} \leq g^0_{\text{SrO}}, \tag{7b}$$

because otherwise TiO_2 or SrO, respectively, would precipitate out of the slab. Combining Eqs. (6) and (4) and the inequalities (7a) and (7b) gives

$$g^0_{\text{TiO}_2} + \Delta G^0_{\text{f,SrTiO}_3} \leq \mu_{\text{TiO}_2} \leq g^0_{\text{TiO}_2}. \tag{8}$$

Therefore at $\mu_{\text{TiO}_2} = g^0_{\text{TiO}_2}$ the system is in equilibrium with TiO_2 and SrTiO_3 and at $\mu_{\text{TiO}_2} = g^0_{\text{TiO}_2} + \Delta G^0_{\text{f,SrTiO}_3}$ the system is in equilibrium with SrO and SrTiO_3.

B. Chemical potential of O_2

We seek an expression for $\mu_{\text{O}_2}(p_{\text{O}_2}, T)$, since p_{O_2} and T are the parameters that can be related most directly to experimental conditions. At temperatures above 300 K and pressures at or below atmospheric, we can use the ideal gas equations to high accuracy if we also make use of experimental thermochemical data to establish the correct reference points for enthalpy and entropy, thereby avoiding errors inherent in first-principles calculations of the free energy at low temperatures. The procedure works as follows. We take as a reference point the chemical potential of oxygen at standard pressure and temperature, $\mu_{\text{O}_2}(p^0, T^0)$, henceforth written as $\mu^0_{\text{O}_2}$, and obtain $\mu_{\text{O}_2}(p_{\text{O}_2}, T)$ by integrating along the pressure and temperature axes in turn. The value of $\mu_{\text{O}_2}(p^0, T^0)$ is obtainable from compilations of thermochemical data, but these work with an energy zero such that oxygen has zero enthalpy in its standard state, whereas our zero of energy is established by the method of first-principles total energy calculation. We nevertheless make use of thermochemical data as much as possible, since they include entropic and quantum statistical terms that we can avoid calculating directly.

1. Calculation of $\mu^0_{\text{O}_2}$

The chemical potential is defined in terms of the enthalpy and entropy per molecule in the standard state by

$$\mu_{\text{O}_2}(p^0_{\text{O}_2}, T^0) \equiv \mu^0_{\text{O}_2} = h^0_{\text{O}_2} - T^0 s^0_{\text{O}_2}. \tag{9}$$

Now the standard enthalpies per molecule of the components in an oxide (for this purpose we first take alumina, but any oxide will do) are related by

$$h^0_{\text{Al}_2\text{O}_3} = 2h^0_{\text{Al}} + \frac{3}{2}h^0_{\text{O}_2} + \frac{1}{N_A}\Delta H^0_{\text{f,Al}_2\text{O}_3}, \tag{10}$$

where $\Delta H^0_{\text{f,Al}_2\text{O}_3}$ is the standard heat of formation per mole and N_A is Avogadro's number. We obtain the value of $\Delta H^0_{\text{f,Al}_2\text{O}_3}$ from the NIST tables of thermochemical data[21] since its value does not depend on the choice of energy zero. The values of $h^0_{\text{Al}_2\text{O}_3}$ and h^0_{Al} are estimated as the total energies per molecule in these crystalline solids, which we have calculated at 0 K. Hence Eq. (10) provides us with the value of $h^0_{\text{O}_2}$. The standard entropy of oxygen $s^0_{\text{O}_2}$ is also obtained directly from tables of thermodynamic data, and combining

TABLE III. Coefficients for enthalpy and entropy expressions in Eqs. (16) and (17) for O_2. [a]

A	29.659	$\times 10^{-3}$	kJ mol^{-1} K^{-1}
B	6.137261	$\times 10^{-6}$	kJ mol^{-1} K^{-2}
C	-1.186521	$\times 10^{-9}$	kJ mol^{-1} K^{-3}
D	0.095780	$\times 10^{-12}$	kJ mol^{-1} K^{-4}
E	-0.219663	$\times 10^3$	kJ mol^{-1} K
F	-9.861391		kJ mol^{-1}
G	237.948	$\times 10^{-3}$	kJ mol^{-1} K^{-1}

[a]Reference 21.

it in (9) with our estimate of $h^0_{\text{O}_2}$ we obtain our required value for $\mu^0_{\text{O}_2}$. An alternative strategy is to take our calculated energies of the solids to be estimates of Gibbs free energies rather than enthalpies. A comparison of the values of $\mu^0_{\text{O}_2}$ obtained from three different oxides, and with both strategies, is shown in Table II. In theory of course the results should be independent of the oxide used, but since we have consistently omitted the thermal energy of the oxides in our calculations, there is some variation of our calculated $\mu^0_{\text{O}_2}$ with oxide and according to whether we assume we are estimating the Gibbs energies or the enthalpies. For subsequent calculations we take the value $\mu^0_{\text{O}_2} = -616$ mRy. The calculated $\mu^0_{\text{O}_2}$ span a range of 16 mRy ≈ 0.2 eV $= 21$ kJ mol^{-1}, so a reasonable estimate of the error in our calculated $\mu^0_{\text{O}_2}$ would be 8 mRy, or 0.1 eV.

2. Integration from $\mu^0_{\text{O}_2}$ to $\mu_{\text{O}_2}(p_{\text{O}_2}, T)$

First, to get to any required pressure p_{O_2} from the reference pressure p^0 (1 atm) at some constant temperature T we can apply the standard thermodynamic relation to a perfect gas,

$$\left. \frac{\partial \mu_{\text{O}_2}}{\partial p} \right|_T = \frac{kT}{p}, \tag{11}$$

where k is Boltzmann's constant, which gives the well-known formula

TABLE IV. Theoretical atomic displacements in Å in the z direction for the SrTiO_2 (001) TiO_2 and SrO terminated surfaces. Positive displacements correspond to a displacement towards the vacuum.

Layer	Atom	TiO_2 termination		SrO termination	
		Ref. 23	Present	Ref. 23	Present
1	Ti	-0.131	-0.1241	-0.220	-0.231
	O	-0.062	-0.0689	$+0.004$	-0.012
2	Sr	$+0.097$	$+0.0906$	$+0.046$	$+0.025$
	O	-0.019	-0.0235	0	-0.018
3	Ti	-0.027	-0.0247	-0.046	-0.047
	O	-0.019	-0.0204	-0.004	-0.010

TABLE V. Atomic displacements in Å for the (2×1) DL-TiO$_2$ surface. A positive value for δz indicates a displacement towards the vacuum. Positive δx is in the direction of left to right in Fig. 3. Erdman *et al.* (Ref. 6) used $a_0 = 3.905$ Å, whereas our lattice constant is the theoretical $a_0 = 3.85$ Å.

Atom	Position	Present results			Ref. 6	
		δx	δz	$\delta z - \delta z^{O13}$	δx	δz^{a}
Ti1	$(1\ \frac{1}{2}\ \frac{5}{2})$	−0.2614	+0.2728	+0.4307	−0.2749[a]	+0.613
Ti2	$(\frac{3}{2}\ 0\ \frac{5}{2})$	+0.1282	+0.1587	+0.3166	+0.1601	+0.398
O1	$(\frac{3}{2}\ \frac{1}{2}\ \frac{5}{2})$	−0.2563	+0.6031	+0.7610	−0.2281	+0.922
O2	$(1\ 0\ \frac{5}{2})$	+0.0215	−0.0628	+0.0951	+0.0226	+0.230
O3	$(0\ 0\ \frac{5}{2})$	−0.0551	−0.0476	+0.1103	−0.0359	+0.168
O4	$(\frac{1}{2}\ \frac{1}{2}\ \frac{5}{2})$	+0.5291	+1.4688	+1.6267	+0.5483	+1.792
Ti3	$(0\ 0\ 2)$	+0.1056	+0.0164	+0.1743	+0.1093	+0.234
Ti4	$(1\ 0\ 2)$	−0.1151	−0.0961	+0.2539	−0.1140	+0.133
O5	$(0\ \frac{1}{2}\ 2)$	+0.0292	−0.2010	−0.0431	+0.0180	−0.027
O6	$(1\ \frac{1}{2}\ 2)$	−0.1841	+0.1235	+0.2813	−0.1788	+0.398
O7	$(\frac{3}{2}\ 0\ 2)$	−0.0098	+0.2274	+0.3853	−0.0055	+0.469
O8	$(\frac{1}{2}\ 0\ 2)$	+0.0032	−0.3436	−0.1858	+0.0008	−0.125
Sr1	$(\frac{3}{2}\ \frac{1}{2}\ \frac{3}{2})$	+0.0652	+0.0530	+0.2109	+0.0719	+0.215
Sr2	$(\frac{1}{2}\ \frac{1}{2}\ \frac{3}{2})$	−0.0804	−0.0481	+0.1097	−0.0758	+0.137
O9	$(1\ 0\ \frac{3}{2})$	+0.2568	+0.0333	+0.1912	+0.2413	+0.246
O10	$(0\ 0\ \frac{3}{2})$	−0.1991	−0.0432	+0.1146	−0.1953	+0.113
Ti5	$(0\ 0\ 1)$	−0.0252	+0.0114	+0.1693	−0.0180	+0.164
Ti6	$(1\ 0\ 1)$	+0.0149	−0.0222	+0.1357	+0.0164	+0.117
O11	$(0\ \frac{1}{2}\ 1)$	+0.0085	−0.0325	+0.1254	+0.0039	+0.102
O12	$(1\ \frac{1}{2}\ 1)$	+0.0014	+0.0430	+0.2008	0.0000	+0.195
O13	$(\frac{3}{2}\ 0\ 1)$	−0.0040	−0.1579	0	−0.0070	0[b]
O14	$(\frac{1}{2}\ 0\ 1)$	+0.0140	+0.1249	+0.2828	+0.0117	+0.277

[a]These are corrected values for the supplementary data published in Ref. 6 obtained from Oliver Warschkow via private communication.

[b]This atom was used as a reference for the *z*-position by Erdman *et al.* (Ref. 6).

$$\mu_{O_2}(p_{O_2}, T) = \mu_{O_2}(p^0, T) + kT \ln\left(\frac{p_{O_2}}{p^0}\right). \qquad (12)$$

This will be sufficiently accurate for a real system under any conditions met in normal experiments. To derive the temperature dependence it is convenient to start from the Gibbs-Helmholtz relation

$$\left.\frac{\partial}{\partial T}\left(\frac{\mu_{O_2}}{T}\right)\right|_p = -\frac{H}{T^2}, \qquad (13)$$

where H is the enthalpy per oxygen molecule. To obtain an expression for H in terms of T we could assume we are dealing with a classical ideal gas, for which

$$H = E_0 + C_p T, \qquad (14)$$

where E_0 is the energy per molecule at 0 K and C_p is the specific heat per molecule at constant pressure, equal to $5k/2$ for a diatomic gas composed of rigid dumbbells. Hence integrating (13) from T^0 to T at constant pressure gives the final expression

$$\mu_{O_2}(p_{O_2}, T) = E_0 + (\mu_{O_2}^0 - E_0)\left(\frac{T}{T^0}\right) - C_p T \ln\left(\frac{T}{T^0}\right)$$
$$+ kT \ln\left(\frac{p_{O_2}}{p^0}\right). \qquad (15)$$

However, this expression still leaves us with the problem of calculating E_0, as well as our uncertainty about the validity of assuming classical rigid dumbbells at all temperatures.
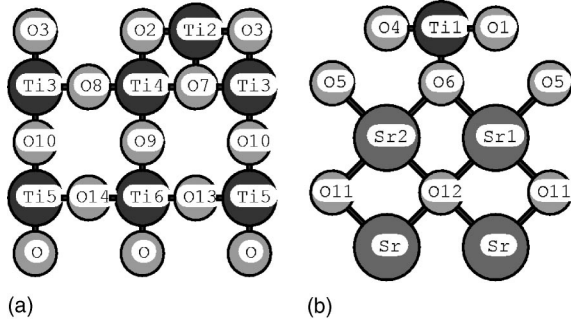
FIG. 3. Vertical slices through (a) TiO$_2$ layer and (b) SrO layer to show atom positions and labels for the (2×1) DL-TiO$_2$ reconstruction.

Rather than attempting to calculate the energy E_0, which would require corrections to the classical formulas for low temperatures, as well as an accurate total energy calculation for the oxygen molecule, we again make use of experimental data. The experimental enthalpies, entropies, and Gibbs free energies per mole have been fitted to polynomials,[21] namely,

$$H(p^0,T) - H(p^0,T^0) = AT + \frac{1}{2}BT^2 + \frac{1}{3}CT^3 + \frac{1}{4}DT^4 - \frac{E}{T} + F,$$

$$(16)$$

$$S(p^0,T) = A\ln(10^{-3}T) + BT + \frac{1}{2}CT^2 + \frac{1}{3}DT^3 - \frac{E}{2T^2} + G,$$

$$(17)$$

and

$$G(p^0,T) = A(T - T\ln(T)) - \frac{1}{2}BT^2 - \frac{1}{6}CT^3$$

$$- \frac{1}{12}DT^4 - \frac{E}{2T} + F - GT, \qquad (18)$$

where the coefficients are listed in Table III.

Note that the data tables give values in kJ mol^{-1}, which we convert to Rydbergs per molecule as necessary. Hence, making use of Eq. (12), we can construct our final formula for $\mu_{O_2}(p_{O_2},T)$:

$$\mu_{O_2}(p_{O_2},T) = \mu_{O_2}(p^0,T^0) + G(p^0,T) - G(p^0,T^0)$$

$$+ kT\ln\left(\frac{p_{O_2}}{p^0}\right). \qquad (19)$$

Equation (19) uses as far as possible the experimental temperature dependence, whereas Eq. (15) was derived by assuming an ideal classical gas of rigid dumbbells. If we fix the value of E_0 by the temperature derivative of the experimental Gibbs energy at the standard temperature, the simple formula Eq. (15) does rather well: the error at 1000 K is only 0.6 kJ mol^{-1}, rising to 3.5 kJ mol^{-1} (<3 mRy) at 2000 K, which is less than other errors in our procedure. However,
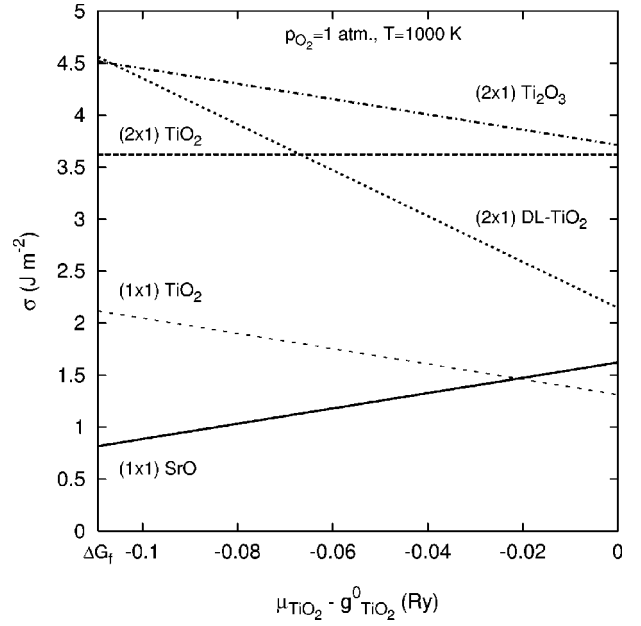

FIG. 4. Surface energies as a function of μ_{TiO_2} at $T=1000$ K and p^0.

we can of course use Eq. (19) directly and avoid any ideal gas assumptions. Either formula tells us that $\mu_{O_2}(p^0,T)$ decreases by 121 mRy between standard temperature (298.15 K) and 1000 K, that is from -616 mRy to -737 mRy.

IV. RESULTS AND DISCUSSION

A. Surface relaxations

For the (1×1) unreconstructed surfaces the calculations were performed on seven atomic layer supercells. The surface energy and atomic displacements are well converged for this size of supercell. Increasing the cell to nine atomic layers only made a difference in the surface energy of 0.05 J m^{-2} for the unrelaxed TiO$_2$ slab. Atomistic relaxation was carried out using a Fletcher-Powell algorithm[22] and the forces were converged to 0.05 mRy au^{-1} for the TiO$_2$ termination and 0.34 mRy au^{-1} for the SrO termination. The results are shown in Table IV.

The agreement between our atomic displacements and those of Ref. 23 is excellent. The only atomic displacements in disagreement are those of the O$_1$ and O$_2$ in the SrO termination.

For the (2×1) reconstructions we used slabs with mirror symmetry about the central layer of the slab. The (2×1) Ti$_2$O$_3$ surface was found to be metallic but nonmagnetic.

The convergence of the surface energy with the thickness of the slabs was checked by comparing the energies for 7 and 11 layer slabs and there was good agreement between the two sets of results. The atomic displacements for the 7 and 11 layer (2×1) DL-TiO$_2$ reconstruction are shown in Table V alongside the previous results reported in Ref. 6. The atom positions are illustrated in Fig. 3. No previous results were available for comparison with the (2×1) TiO$_2$ or (2×1)
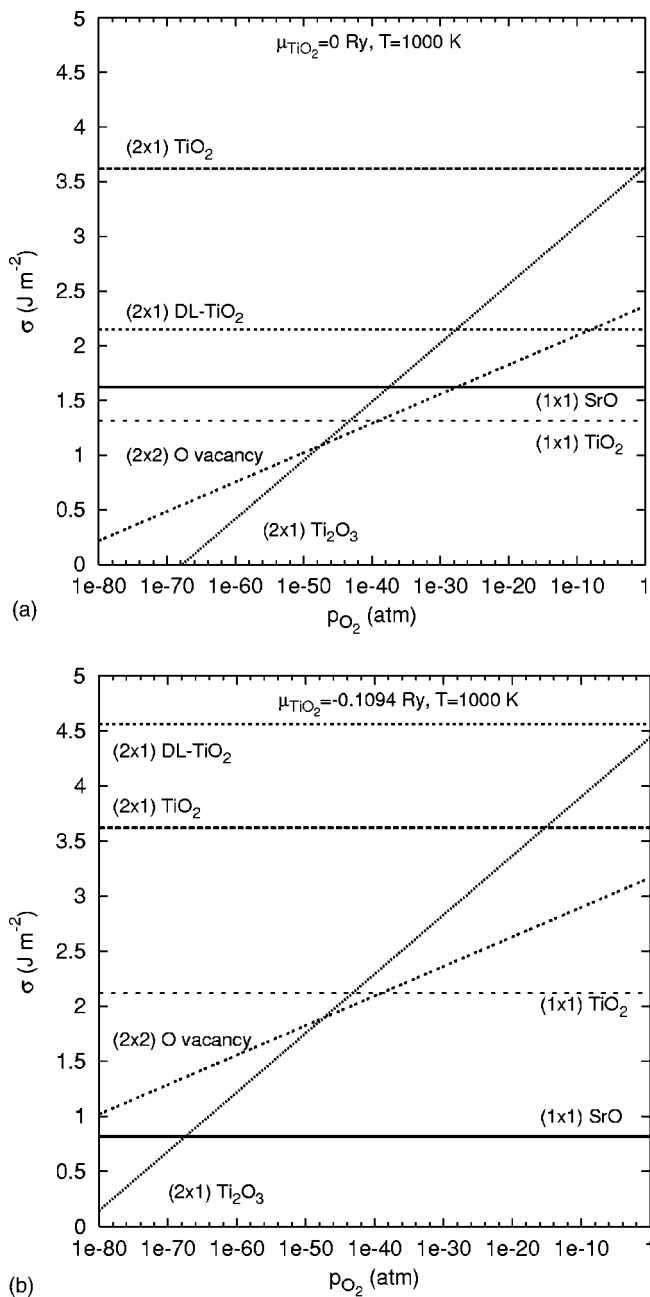
(a)

(b)

FIG. 5. Surface energies as a function of p_{O_2} at $T=1000$ K (a) in equilibrium with TiO$_2$ and (b) in equilibrium with SrO.

FIG. 6. STM image (2 V sample bias, 0.5 nA tunneling current) of the (2$\times$1) reconstructed surface. The two unit cell separation of the rows can be seen, but the single unit cell periodicity along the rows is not resolved. The (2$\times$1) surface unit cell is shown in the image. By averaging vertically through the image a plot of the average row heights is created as shown in the lower panel. The typical corrugation height is between 0.4 and 0.5 Å.

B. Surface energies

The surface energies of the (1$\times$1) and (2$\times$1) reconstructed surfaces as a function of μ_{TiO_2} are shown in Fig. 4. As expected from the theory, Eq. (3), the gradient of each energy is proportional to the excess of TiO$_2$ subunits. The (2$\times$1) TiO$_2$ surface has the same stoichiometry as the bulk and therefore is independent of μ_{TiO_2}.

The surface energies of the (1$\times$1) unreconstructed surfaces are in good agreement with previous theory. The average surface energy of these terminations is 1.46 J m^{-2} which compares well to previous values, for example 1.35 J m^{-2}.[23]

Surprisingly the (1$\times$1) surfaces are more stable than any of the (2$\times$1) reconstructions at p^0 and $T=1000$ K. As previously stated in the introduction one likely explanation is that the (1$\times$1) unreconstructed surfaces are not stable in an UHV experiment. To test this hypothesis we have calculated the surface energy of the (1$\times$1) TiO$_2$ terminated surface with an oxygen vacancy. For this surface we used a supercell with a (2$\times$2) unreconstructed TiO$_2$ terminated surface with 7 atomic layers and one layer of vacuum and it will be referred to as the (2$\times$2) O vacancy surface. Similar to the (2$\times$1) Ti$_2$O$_3$ reconstruction this surface is metallic.

Only the surface with the O vacancy and the (2$\times$1) Ti$_2$O$_3$ surface energies depend on p_{O_2} and T since they are the only surfaces with an excess of oxygen (in these cases a negative excess or deficiency). Figures 5(a) and 5(b) show σ vs p_{O_2} at $T=1000$ K for two different values of μ_{TiO_2} corresponding to equilibrium with TiO$_2$ and SrO, respectively.

First we consider the case where the surface is in equilibrium with SrO. The DL-TiO$_2$ and (2$\times$1) TiO$_2$ reconstructions and the (1$\times$1) TiO$_2$ surface with and without an O vacancy are unstable for all values of p_{O_2} shown. The (1

Ti$_2$O$_3$ reconstructions. The following results for the (2$\times$1) reconstructions were obtained using slabs with 11 atomic layers.

The agreement between our results and those of Ref. 6 is excellent. The direction of all displacements are consistent although there is some variation of magnitude. For both sets of results the Ti1-O4 bond length is considerably shorter that the bulk equilibrium bond length. Erdman *et al.* obtained a bond length of 1.63 Å and we obtained a bond length of 1.64 Å. The angle between the Ti1-O4 bond and the (001) plane are also in remarkable agreement. Erdman *et al.* obtained a bond angle of 46.2° and we obtained an angle of 46.5°.
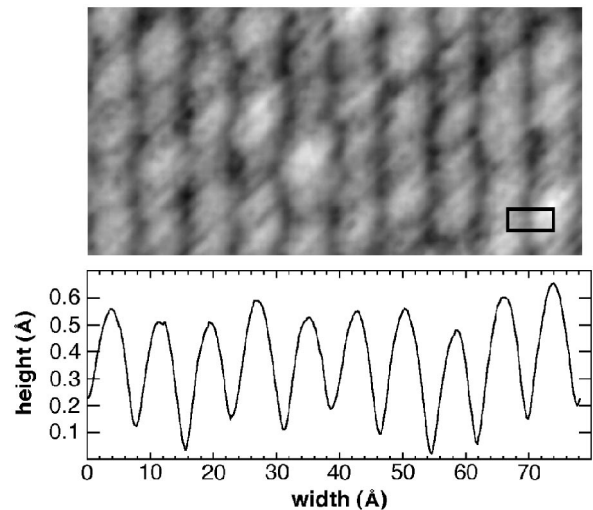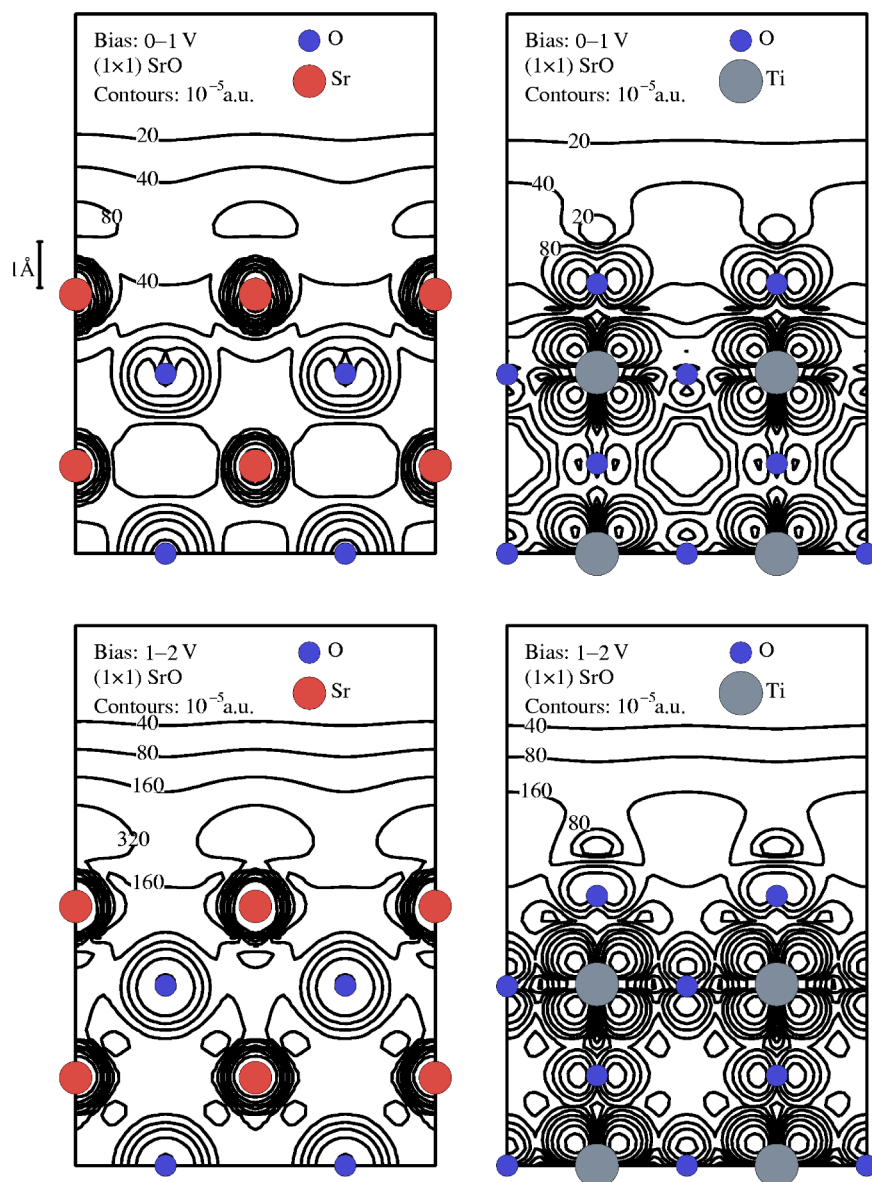
FIG. 7. (Color online) Charge densities for the (1×1) SrO terminated surface for slices through the SrO and TiO$_2$ planes in two different energy windows above the conduction band.

$\times 1$) SrO terminated surface is predicted to be stable for partial pressures down to $\approx 10^{-68}$ atm at which point the (2×1) Ti$_2$O$_3$ surface becomes stable. If we assume that the ideal (1×1) surface is never obtained then the (2×2) O vacancy surface has the lowest surface energy for partial pressures down to $\approx 10^{-48}$ atm after which the (2×1) Ti$_2$O$_3$ reconstruction is again stable.

Now we consider the case where the surface is in equilibrium with TiO$_2$. For partial pressures above $\approx 10^{-40}$ the perfect (1×1) TiO$_2$ unreconstructed surface is stable. Neglecting, for now, the apparent overall stability of the (1×1) surfaces then for $p_{O_2} > 10^{-8}$ the DL-TiO$_2$ surface is stable, for $10^{-48} < p_{O_2} < 10^{-8}$ the (2×2) O vacancy surface is stable, and for $10^{-68} < p_{O_2} < 10^{-48}$ the (2×1) Ti$_2$O$_3$ reconstruction is stable.

The pressures under consideration here are not achievable experimentally. However, it is possible to obtain extremely low *effective* partial pressures if a reducing agent is present. To estimate the effective partial pressures which could be obtained we have taken as an example the case of carbon being present on the surface. Consider the thermodynamic equation for the formation of carbon dioxide from carbon and oxygen at standard temperature $T^0 = 298$ K,

$$C_{(s)} + O_{2(g)} \rightleftharpoons CO_{2(g)},$$
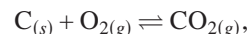
where carbon is in graphite form and CO$_2$ and O$_2$ are in the gas phase. The Gibbs free energy balance at standard temperature and pressure is

$$\mu^0_{CO_2} = \mu^0_C + \mu^0_{O_2} + \Delta G_{f,CO_2}, \tag{20}$$

where $\Delta G_{f,CO_2}$ is the Gibbs free energy of formation of carbon dioxide at standard temperature and pressure. In equilibrium

$$\mu_{CO_2}(p,T) = \mu_C(p,T) + \mu_{O_2}(p,T) \tag{21}$$

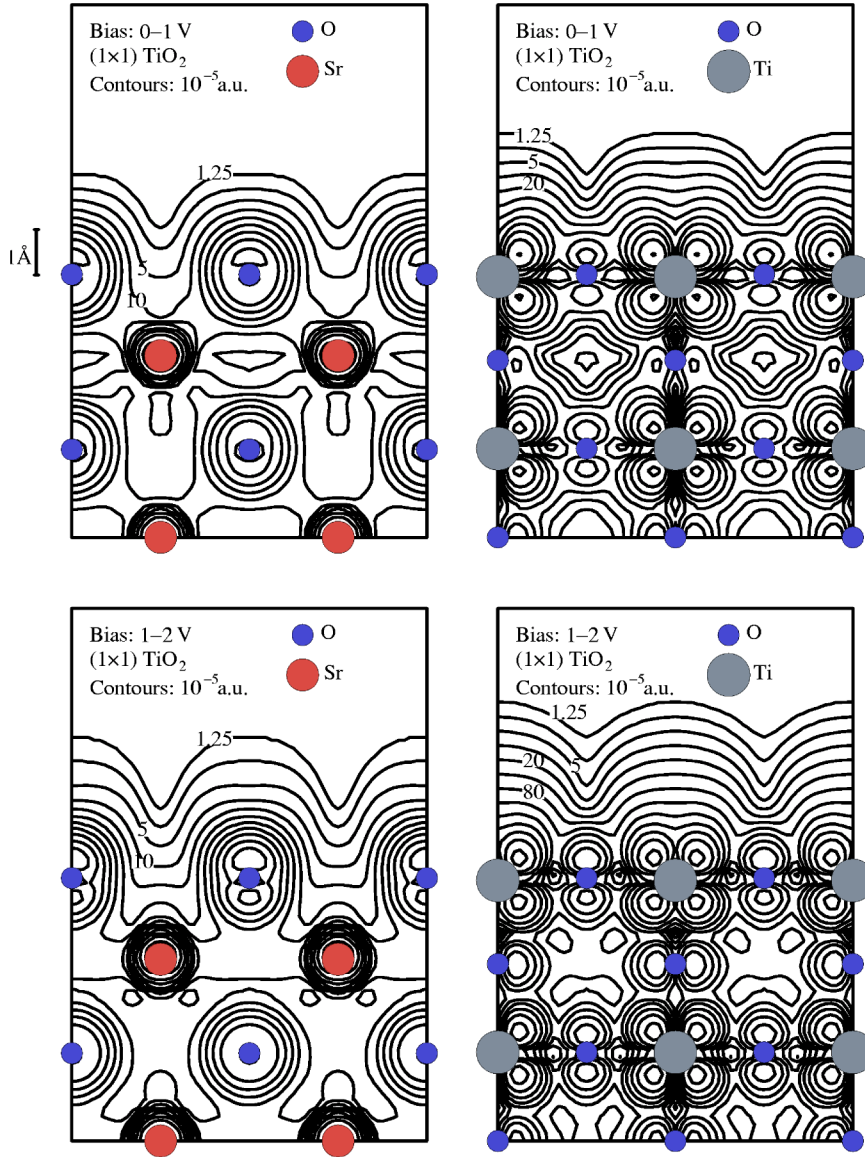and using the earlier derivation for the pressure dependence of the chemical potential of oxygen we can write

FIG. 8. (Color online) Charge densities for the (1×1) TiO$_2$ terminated surface for slices through the SrO and TiO$_2$ planes in two different energy windows above the conduction band.

$$\mu_{\text{CO}_2}(p^0,T) + RT \ln\left(\frac{p_{\text{CO}_2}}{p^0}\right) = \mu_{\text{C}}(p,T) + \mu_{\text{O}_2}(p^0,T)$$

$$+ RT \ln\left(\frac{p_{\text{O}_2}}{p^0}\right). \quad (22)$$

Subtracting Eq. (20) from Eq. (22) at $T^0 = 298$ K gives

$$RT^0 \ln\left(\frac{p_{\text{CO}_2}^0}{p_{\text{O}_2}}\right) = -\Delta G_{\text{f,CO}_2}. \quad (23)$$

At standard temperature $RT^0 = 0.592$ kcal, $\Delta G_{\text{f,CO}_2}$ $= -94.15$ kcal,[21] and if the partial pressure of CO$_2$ corresponds to UHV pressures ($\approx 10^{-15}$ atm), then p_{O_2} $\approx 10^{-85}$ atm. This simple analysis demonstrates that it is possible to achieve low partial pressures if a reducing agent is present. In Castell's experiment a chemical etch was used to prepare the surface and this is known to leave a carbon residue. This etch also serves to produce a TiO$_2$ rather than SrO

termination so Fig. 5(a) is the most appropriate to compare to these experiments. Although the surface is annealed to remove this layer it is possible that some carbon remains which may reduce the effective partial pressure of oxygen enough to enable the (2×1) Ti$_2$O$_3$ reconstruction to become stable.

V. IMAGE SIMULATIONS AND STM IMAGES

The question as to why the (1×1) unreconstructed surfaces have not been observed has not yet been answered. In this section we look at the unoccupied charge densities and make comparisons with STM imaging.

Figure 6 shows an STM image of the (2×1) reconstructed surface. The sample bias is positive so that electrons tunnel from the metallic STM tip into the unoccupied states of the SrTiO$_3$ specimen. The details of sample preparation and imaging conditions are the same as those described in Ref. 4. In the lower panel of Fig. 6 a plot of the average row
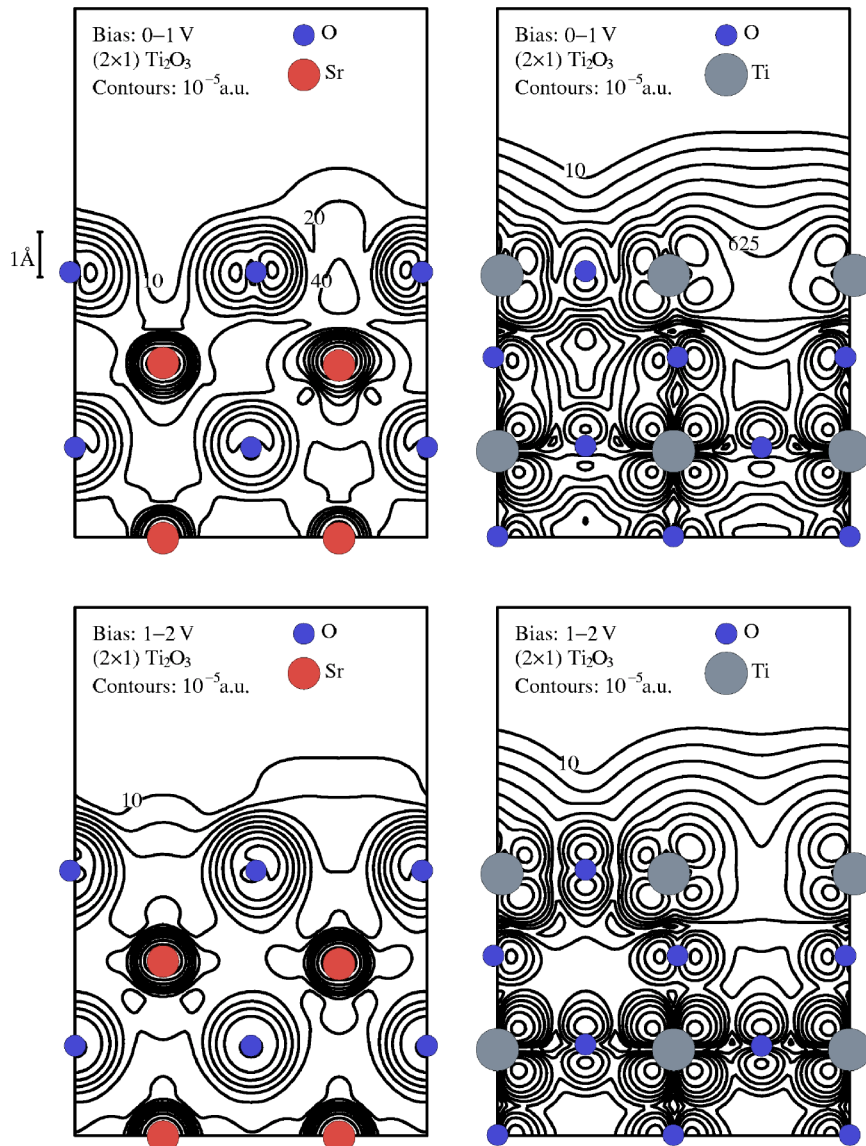
FIG. 9. (Color online) Charge densities for the (2×1) Ti_2O_3 terminated surface for slices through the SrO and TiO_2 planes in two different energy windows above the conduction band.

height is shown. This plot shows in particular that the corrugation height perpendicular to the rows in the image is between 0.4 and 0.5 Å. The unit cell periodicity parallel to the rows cannot be resolved in the STM images.

A popular method for STM image analysis is to integrate the local density of states in an energy window around the imaging bias voltage. This method was used most notably on rutile TiO_2 (110) surfaces[24] and has since been applied to other oxide surfaces, e.g., NiO and CoO.[9] In our study we have integrated the empty states over two energy windows and compared the results. The windows considered, measured upwards from the conduction band edge, were $0-1$ eV and $1-2$ eV.

A. (1×1) unreconstructed surfaces

Figures 7 and 8 show the unoccupied charge densities of the (1×1) SrO and TiO_2 surfaces with slices through the SrO and TiO_2 planes.

The difference between the charge densities in the two different energy windows is not significant therefore the re-sults should not be sensitive to the sample bias.

It is interesting to note that the charge density for the SrO surface is an order of magnitude larger than that of the TiO_2 surface. Even though for both surfaces the charge density around the Sr ions is much higher than around the Ti ions the contours of constant charge density on the (1×1) SrO surface are flatter than for the (1×1) TiO_2 surface. The high charge density around the Sr ions is in agreement with the findings of Kubo and Nozoye's[8] calculations of their Sr adatom model. The charge density plots would therefore suggest that it is easier to obtain atomic resolution STM images from the (1×1) TiO_2 surface than from the (1×1) SrO surface. Experimental conditions such as sample bias and tunneling current would determine which charge density contours are imaged in the STM.

B. (2×1) reconstructions

Figures 9 and 10 show the charge densities of the (2×1) Ti_2O_3 and DL-TiO_2 surfaces. As for the (1×1) re-
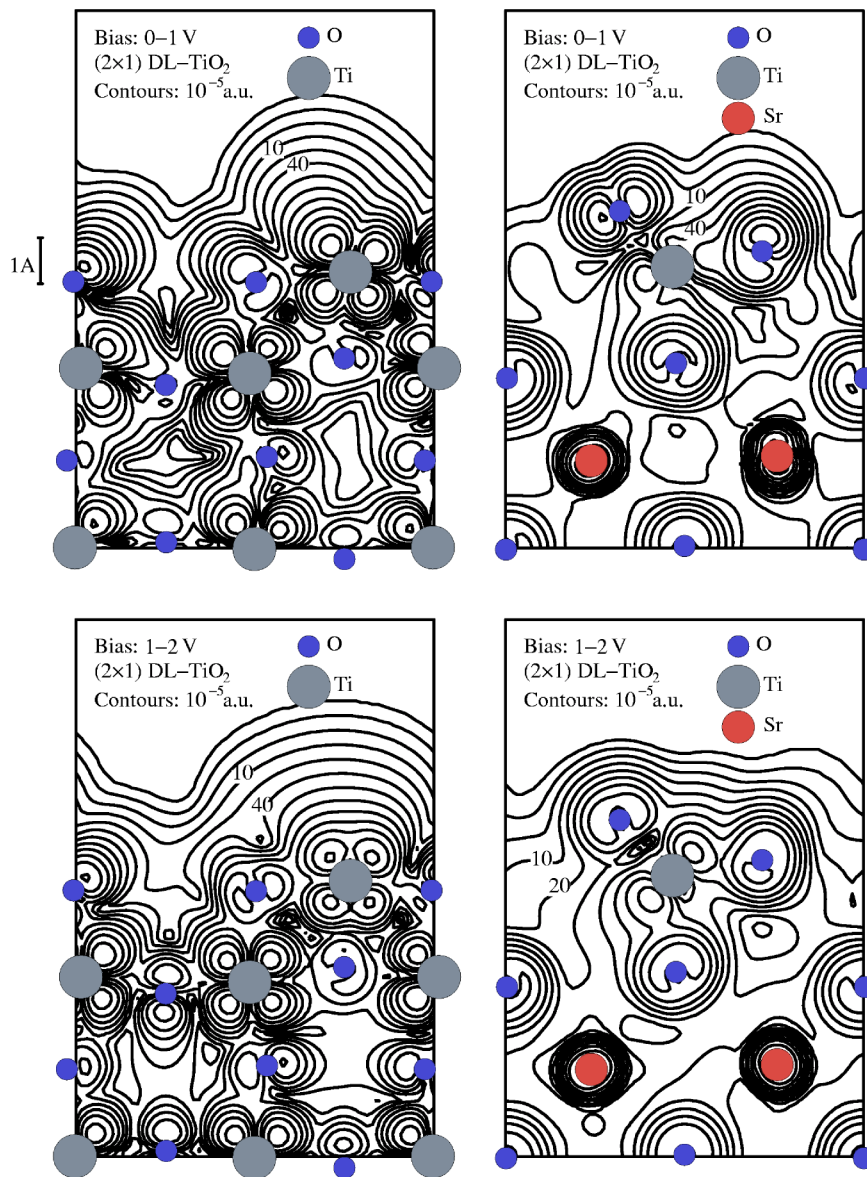
FIG. 10. (Color online) Charge densities for the (2×1) DL-TiO$_2$ terminated surface for slices through the SrO and TiO$_2$ planes in two different energy windows above the conduction band.

constructions two different energy windows and slices through the SrO and TiO$_2$ planes are shown. The (2×1) TiO$_2$ surface has not been considered here because its surface energy is higher than the others.

The charge density for the Ti$_2$O$_3$ is different in the two energy windows for the slice through the SrO layer. In the $0-1$ eV window the corrugation is significantly larger than for the $1-2$ eV window. Even so, the corrugation in both cases should be large enough to be imaged using STM. Surprisingly, the charge density of the Ti$_2$O$_3$ surface is higher over the missing O row which indicates that the missing rows would be imaged rather than the rows of O atoms.

The relaxation of DL-TiO$_2$ surface can be clearly seen in Fig. 10 including the remarkably short Ti-O bond length. In this case the regions of high charge density occur over the atoms, rather than over the missing atoms. The charge density contours of the (2×1) DL-TiO$_2$ surface are highly irregular and it should therefore be possible to image them in the STM. However, the large corrugations one sees in Fig. 10 would not be reproduced in experiment due to the convolu-

tion of the STM tip with the sample which would have the effect of reducing the corrugation heights.

The calculations show that the STM images the missing atoms for the (2×1) Ti$_2$O$_3$ reconstruction and atomic positions for the (2×1) DL-TiO$_2$. If one were to adsorb a molecule that attaches to the middle of the rows for both structures then it would be possible to distinguish the structures because in the STM images the (2×1) Ti$_2$O$_3$ surface would show the molecule in between bright rows and the (2×1) DL-TiO$_2$ surface would show it on top of the bright rows. This highlights the significance of the very different nature of the charge densities for the two proposed (2×1) reconstructions.

VI. CONCLUSIONS

We have performed first-principles total energy calculations for several (2×1) reconstructions of the (001) SrTiO$_3$ surface. The surface energies were calculated as functions of μ_{TiO_2}, p_{O_2}, and T.

At standard pressure p^0 and $T=1000$ K the (1×1) surfaces are energetically stable and all the (2×1) reconstructions are unstable. The (2×1) TiO_2 reconstruction is unstable under all the conditions considered. Under conditions of very low p_{O_2} the (2×1) Ti_2O_3 reconstruction is stable.

Charge densities for the reconstructions were calculated to investigate why the (1×1) surfaces have not been observed using STM despite the fact that they are predicted to be stable under many conditions. Of the two (1×1) surfaces the TiO_2-terminated surface should be easier to image than the SrO-terminated surface. The corrugations of the charge density for the (2×1) surfaces are deeper than those for the (1×1) surfaces and therefore the (2×1) reconstructions should be easier to image than the (1×1).

We considered the possibility that the ideal (1×1) surfaces considered here do not exist in practice. In UHV conditions it is likely that oxygen vacancies are present. A calculation of the (2×2) O vacancy surface shows that the vacancy raises the surface energy of the (1×1) surface and in some conditions it becomes higher than that of the (2×1) reconstructed surfaces. In a TiO_2-rich environment with oxygen partial pressure greater than 10^{-8} atm its surface energy is greater than that of the (2×1) DL-TiO_2 reconstruction and so this reconstruction becomes the stable one.

In this analysis, there has been no consideration of vibrational entropy. Surface vibrations could contribute to the lowering of the energy. In particular, the "dangling" oxygen atoms in the DL-TiO_2 surface could give rise to low frequency surface vibrations which could stabilise this reconstruction.

Recently Kubo and Nozoye[8] suggested that all the observed reconstructions could be explained using a Sr-adatom model. However no total energy calculations were carried out and without these it is impossible to compare these surface structures with the previous structures proposed. It would be interesting to carry out a total energy calculation of these surfaces and this may shed light on the unresolved issues.

*Present address: Department of Physics and Astronomy , Rutgers University, Piscataway, New Jersey 08854.

†Permanent address: Department of Materials, University of Oxford, Parks Road, Oxford OX1 3PH, United Kingdom.

[1] V. E. Henrich and P. A. Cox, *The Surface Science of Metal Oxides*, 1st ed. (Cambridge University Press, Cambridge, 1994).

[2] Q. D. Jiang and J. Zegenhagen, Surf. Sci. **338**, L882 (1995).

[3] T. Kubo and H. Nozoye, Phys. Rev. Lett. **86**, 1801 (2001).

[4] M. R. Castell, Surf. Sci. **505**, 1 (2002).

[5] M. R. Castell, Surf. Sci. **516**, 33 (2002).

[6] N. Erdman, K. R. Poeppelmeier, M. Asta, O. Warschkow, D. E. Ellis, and L. D. Marks, Nature (London) **419**, 55 (2002).

[7] N. Erdman and L. D. Marks, Surf. Sci. **526**, 107 (2003).

[8] T. Kubo and H. Nozoye, Surf. Sci. **542**, 177 (2003).

[9] M. R. Castell, S. L. Dudarev, G. A. D. Briggs, and A. P. Sutton, Phys. Rev. B **59**, 7342 (1999).

[10] M. Methfessel and M. van Schilfgaarde, NFP Manual (1997), unpublished.

[11] *Electronic Structure and Physical Properties of Solids: The Uses of the LMTO Method; Lectures of a Workshop held at Mont Saint Odile*, edited by H. Dreyssé (Springer-Verlag, Berlin 2000), pp. 114–147.

[12] A. T. Paxton and L. Thiên-Nga, Phys. Rev. B **57**, 1579 (1998).

[13] D. Singh, Phys. Rev. B **43**, 6388 (1991).

[14] R. D. King-Smith and D. Vanderbilt, Phys. Rev. B **49**, 5828 (1994).

[15] Y. Furuhata, E. Nakamura, and E. Sawaguchi, Landolt-Börnstein, Group III 3 (1969).

[16] R. O. Bell and G. Rupprecht, Phys. Rev. **129**, 90 (1963).

[17] M. W. Finnis, Phys. Status Solidi A **166**, 397 (1998).

[18] I. G. Batyrev, A. Alavi, and M. W. Finnis, Phys. Rev. B **62**, 4698 (2000).

[19] A. Y. Lozovoi, A. Alavi, and M. W. Finnis, Comput. Phys. Commun. **137**, 174 (2001).

[20] J. Padilla and D. Vanderbilt, Phys. Rev. B **56**, 1625 (1997).

[21] *NIST Chemistry WebBook, NIST Standard Reference Database Number 69*, edited by P. J. Linstrom and W. G. Mallard, (National Institute of Standards and Technology, Gaithersburg, MD, 2003), 20899 http://webbook.nist.gov/chemistry/.

[22] R. Fletcher and M. Powell, Comput. J. **6**, 163 (1963).

[23] J. Padilla and D. Vanderbilt, Surf. Sci. **418**, 64 (1998).

[24] U. Diebold, J. F. Anderson, K.-O. Ng, and D. Vanderbilt, Phys. Rev. Lett. **77**, 1322 (1996).